CrossMark

Thermoanalytical (TG/DSC/EVG–GC–MS) characterization of the lanthanide (Ho) iron garnet formation in sol–gel

Thermal process

Olga Opuchovic[1] · Daniel Niznansky[2] · Aivaras Kareiva[1]

Abstract In the present study, the investigation of formation mechanism of holmium iron garnet ($Ho_3Fe_5O_{12}$, HoIG) prepared by an aqueous sol–gel method was reported. We specifically focused on the identification of species released during the thermal decomposition of the Ho–Fe–O precursor gel using thermal analysis method. The formation of holmium iron garnet phase and some magnetic properties were investigated by X-ray diffraction analysis, Mössbauer spectroscopy and TG–DSC measurements. Evolved gas analysis of the decomposition products of gel precursor was performed by coupled TG–GC–MS method. In addition, the Curie temperatures of series of rare earth iron garnets were measured using thermal analyser with the small permanent magnet. The influence of the transition temperature from ferrimagnetic to paramagnetic state on the nature of lanthanide element in the iron garnets has been also investigated.

Keywords Holmium iron garnet · Sol–gel processing · Formation mechanism · TG–DSC · TG–GC–MS · Curie temperature

✉ Olga Opuchovic
olga.opuchovic@chf.vu.lt

1 Department of Inorganic Chemistry, Vilnius University, Naugarduko 24, 03225 Vilnius, Lithuania

2 Department of Inorganic Chemistry, Faculty of Science, Charles University in Prague, Hlavova 2030/8, 12843 Prague 2, Czech Republic

Introduction

Over the past few decades, magnetic materials have been in focus of interest due to the fact that they are widely used in modern technology [1]. It is well known that based on the behaviour under an applied external magnetic field the materials can be classified into the following five groups: diamagnetic, paramagnetic, antiferromagnetic, ferromagnetic and ferrimagnetic [2]. Ferromagnetic and ferrimagnetic materials on the basis of their hysteresis characteristics are classified as either soft or hard [3]. Soft ferrites can be used for high-frequency applications, such as power supplies, chokes and antenna, and for microwave isolators, circulators, phase shifters, filters, while permanent magnets are used in electric motors, generators and actuators [4]. Basic magnetic properties that let us to consider materials as soft or hard are remanence (B_r), coercive force (H_c) and Curie temperature (T_c) [5].

Curie temperature is important for the practical applications of magnetic materials and can be determined by thermal analysis technique [6, 7]. Temperature calibration of the thermal analyser is usually performed by means of the Curie temperatures of known ferromagnetic materials. The total downward force on the sample at temperatures below the Curie point is the sum of the sample weight and the magnetic force [8]. The ferromagnetic or ferrimagnetic materials at T_c become paramagnetic (magnetic force is reduced to zero), and a sudden loss or increase in apparent mass appears [9, 10]. At this temperature, another important magnetic parameter, called saturation magnetization (M_s), falls rapidly to zero [7].

Ferrimagnetic rare earth iron garnets belong to the class of soft magnetic materials [11]. These materials are easily magnetized and demagnetized [2, 5]. This behaviour is related to the magnetic domains, while magnetic domain is

the region where the atomic magnetic moments are aligned [2]. The control of magnetic domains is the key in obtaining desirable magnetic properties. The magnetization–demagnetization behaviour is a function of domain wall mobility, which is controlled by the final microstructure of the compound. This means that size, shape and orientation of the crystallites or grains, as well as the presence of any second-phase particles in the sample, can influence this behaviour. On the other hand, the microstructure of crystalline material depends very much on the method of preparation [3].

Rare earth iron garnets have been produced in various ways and forms [1, 12–18]. Understanding the formation mechanism of the product is important to precisely control all previously mentioned properties of these materials in order to generate dependable structure–property correlations. Sol–gel synthesis process is attractive for the preparation of homogeneous materials with controlled structure–property characteristics [19]. Thermal analysis combined with evolved gas analysis has been used for the characterization of the precursor gels in the systems of ZrO_2–CeO_2 [20], ZrO_2 [21], TiO_2 [22] and Y–Fe–O nanopowders [23]. This technique allows us to study the conversion of the gel to the densified powders. Thermogravimetry (TG) coupled with gas chromatography and mass spectroscopy (GC–MS) makes it possible to determine gaseous species evolved during the thermal decomposition process [24]. Advanced thermoanalytical techniques can give the deeper understanding of the structure of the xerogels obtained by sol–gel method and the formation of densified ceramics from the gel. Controlling and understanding the synthesis process is promising for the obtaining desirable properties of the materials.
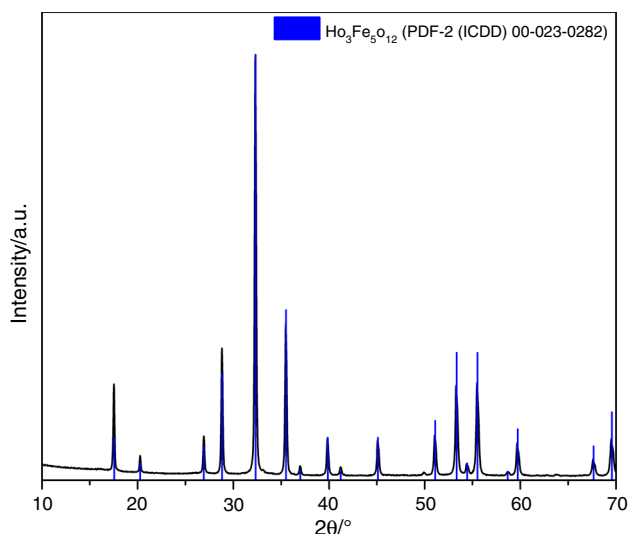

Fig. 1 XRD pattern of Ho–Fe–O precursor gel heated at 800 °C. *Vertical lines* represent standard XRD pattern of $Ho_3Fe_5O_{12}$
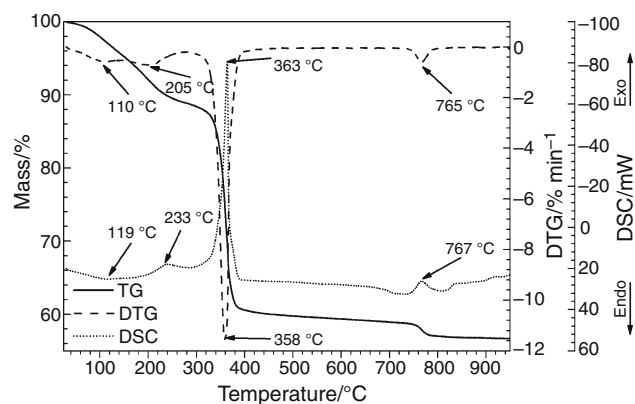

Fig. 2 TG/DTG/DSC curves of the Ho–Fe–O precursor gel under flowing air

The aim of this work was to investigate the formation process of holmium iron garnet from the Ho–Fe–O precursor gel by using thermal analysis technique. The investigation of the Curie temperature changes in the series of lanthanide iron garnets was one of the purposes of this study as well.

Experimental

Materials and synthesis

Holmium iron garnet sample was prepared by an aqueous sol–gel method as reported previously [25]. Iron (III) nitrate nonahydrate ($Fe(NO_3)_3 \cdot 9H_2O$, 98.0% Duro-Galvanit-Chemie) and holmium oxide (Ho_2O_3, 99.9% Aldrich) were used as starting materials. Holmium oxide was dissolved in hot nitric acid (HNO_3, 65% Eurochemicals) under stirring. The excess of acid was removed by evaporation till the dry residue. In the following step, 20 mL of
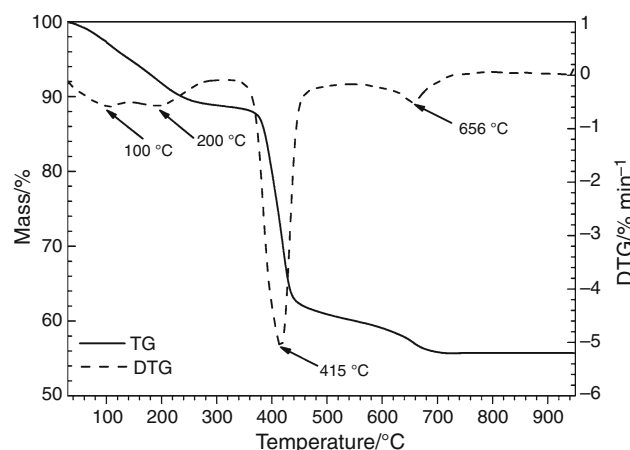

Fig. 3 TG/DTG curves of the Ho–Fe–O precursor gel under flowing nitrogen

deionized water was added and clear solution was obtained. $Fe(NO_3)_3 \cdot 9H_2O$ was dissolved in 50 mL of deionized water, and both solutions were mixed. After stirring it for 1 h at 55–65 °C, the complexing agent 1,2-ethanediol ($C_2H_6O_2$, 99.5% Aldrich) was added to this solution in the molar ratio of 1:1 to the total metal ions. After stirring for 1 h, obtained solutions were evaporated to form gels. The synthesized gels were dried in an oven (120 °C) for 24 h. The obtained dry xerogels were ground to fine powders and preheated at 800 °C for 2 h at a heating rate of 10 °C min^{-1}. Then, powders were additionally sintered for 10 h. All other polycrystalline lanthanide iron garnet powders were prepared analogously by the same aqueous

sol–gel method [25]. The HoIG synthesized at 800 °C was used for more detailed analysis. Individual Fe–O and Ho–O gels were synthesized separately to investigate the formation of the mixed-metal oxide. These individual gels were prepared by the same procedure as Ho–Fe–O precursor.

Characterization

X-ray diffraction (XRD) measurements were performed on PANalytical X'Pert PRO diffractometer with secondary monochromator and PIXcel position-sensitive detector using CuK$_\alpha$ radiation. The data were collected within 2θ angle from 5° to 70° at a step size of 0.026°.

Fig. 4 Gas chromatographic elutions of the gas phase evolved at 415 °C (*top*) and 656 °C (*bottom*) of Ho–Fe–O gel under flowing nitrogen. Mass spectra recorded corresponding to selected chromatographic peaks (TG–GC–MS analysis)
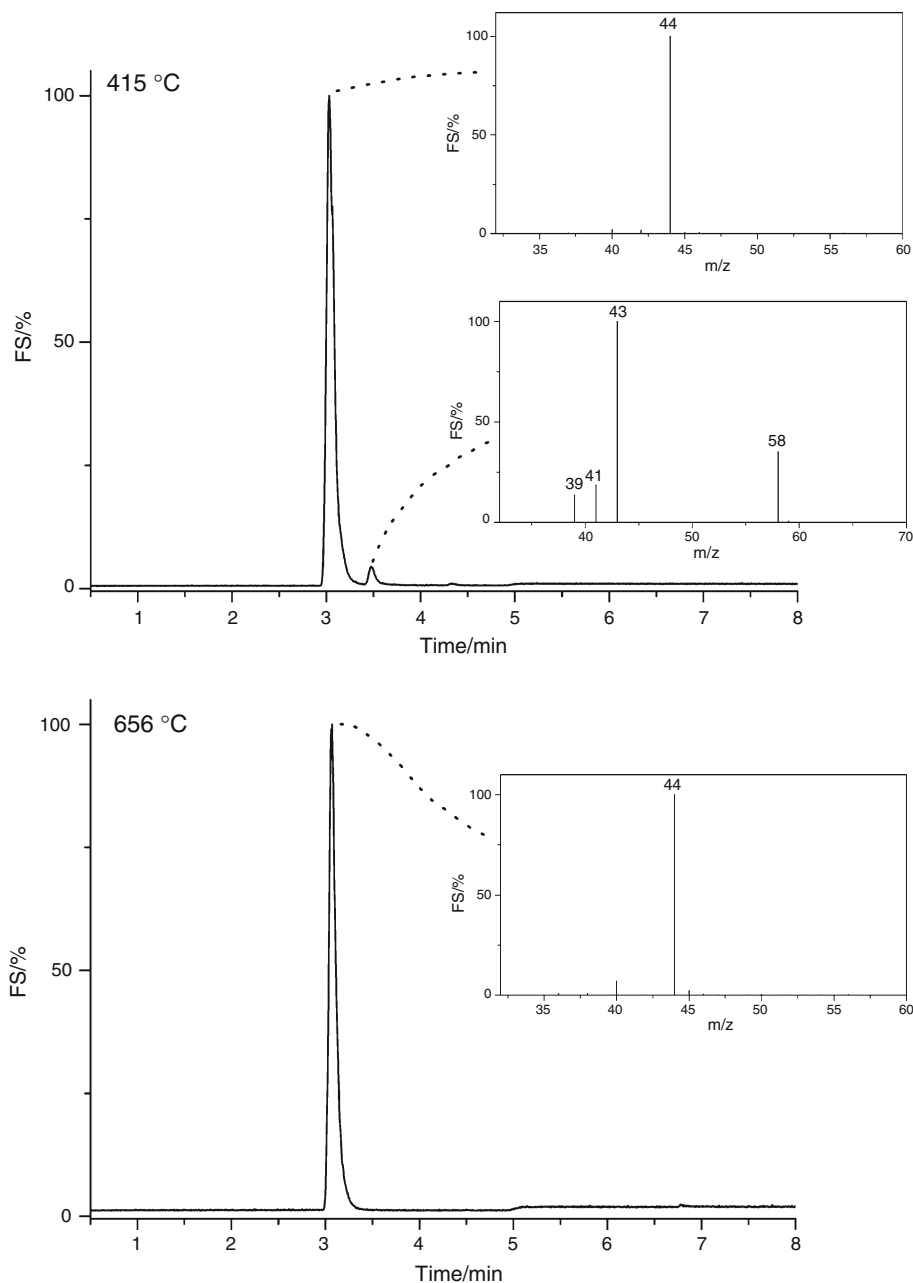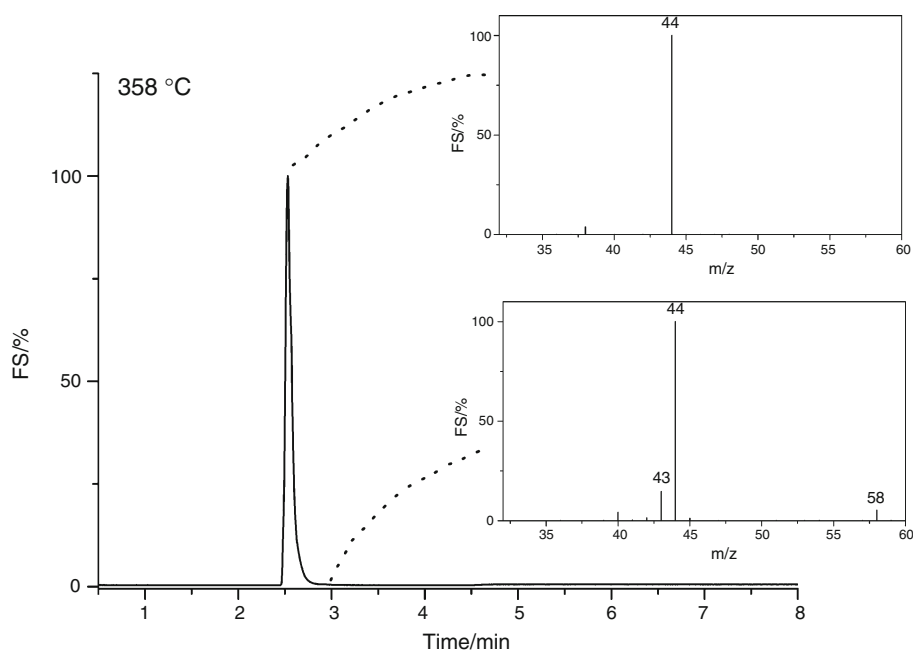
Fig. 5 Gas chromatographic elutions of the gas phase evolved at 358 °C of Ho–Fe–O gel under flowing air. Mass spectra recorded corresponding to selected chromatographic peaks (TG–GC–MS analysis)

Thermogravimetric and differential scanning calorimetry (TG–DSC) measurements were performed under 20 mL min^{-1} of flowing air at a heating rate of 10 °C min^{-1} using Simultaneous Thermal PerkinElmer analyzer STA6000. Around 10 mg of powdered samples was analysed using alumina crucible. Coupled TG–GC–MS analysis was used for the determination of the evolved gases at different temperatures. Thermogravimetric analysis (TG, DTG) was performed using Pyris 1 TGA thermal analyser from PerkinElmer and carried out under 20 mL min^{-1} of nitrogen and air flow at a heating rate of 10 °C min^{-1}. About 5–10 mg of samples was analysed using platinum crucible. Gas analyses were performed on a PerkinElmer Clarus 600 gas chromatograph using Elite-5MS capillary column (30 m, 0.25 mm) and He as a carrier gas with temperature program: 35 °C for 5 min followed by 10 °C min^{-1} heating up to 200 °C for 5 min. Injections of gas sample were done for temperatures corresponding to the most important mass losses on the DTG curve. Gas fractions were gas chromatographically eluted before mass spectroscopic detection. The evolved gases were determined on the basis of their mass spectra. Mass spectrometric analyses were recorded with a quadrupole mass spectrometer. Electron impact (70 eV) mass spectra were recorded from 35 to 350 m/z. Mössbauer spectra were measured in transmission mode with ^{57}Co diffused into Rh matrix as the source moving with constant acceleration. The spectrometer was calibrated by means of a standard α-Fe foil, and the isomer shift was expressed with respect to this standard at 293 K. The samples were measured at the temperature of 293 K. The fitting of the spectra was performed with the help of the NORMOS programme. A

thermogravimetric device with the small magnet was adapted to determine Curie temperature of series of rare earth iron garnets. Measurements were performed from 200 to 360 °C with the heating rate of 5 °C min^{-1} under 20 mL min^{-1} of flowing nitrogen. Analysis was performed with 10–12 mg of sample using platinum crucible.

Results and discussion

Formation of the garnet phase

Figure 1 shows the XRD pattern recorded for Ho–Fe–O precursor gel annealed at 800 °C. The reference pattern of Ho$_3$Fe$_5$O$_{12}$ (PDF-2 (ICDD) 00-023-0282) is also added. It
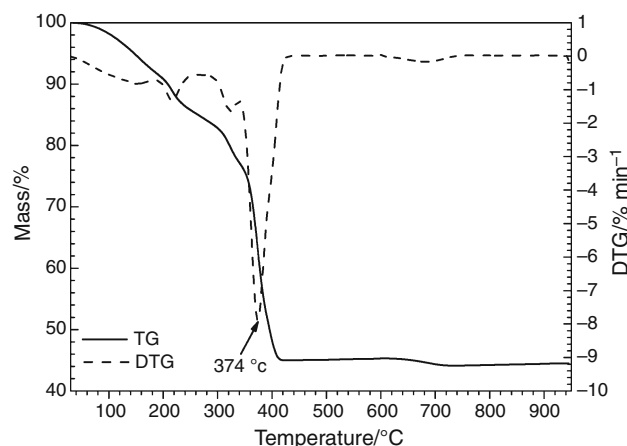

Fig. 6 TG/DTG curves of the Fe–O precursor gel under flowing nitrogen

Fig. 7 Gas chromatographic elutions of the gas phase evolved at 374 °C of Fe–O gel under flowing nitrogen. Mass spectra recorded corresponding to selected chromatographic peaks (TG–GC–MS analysis)
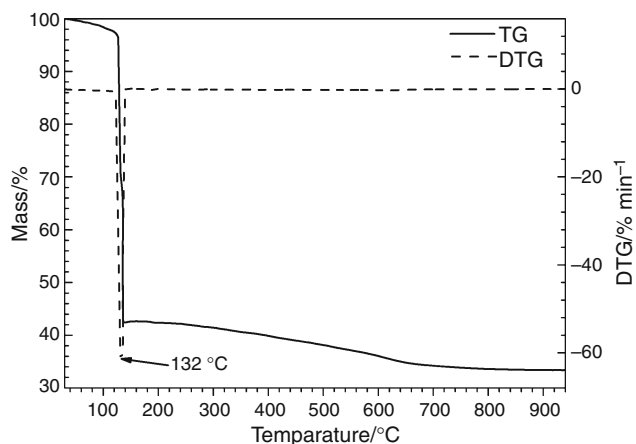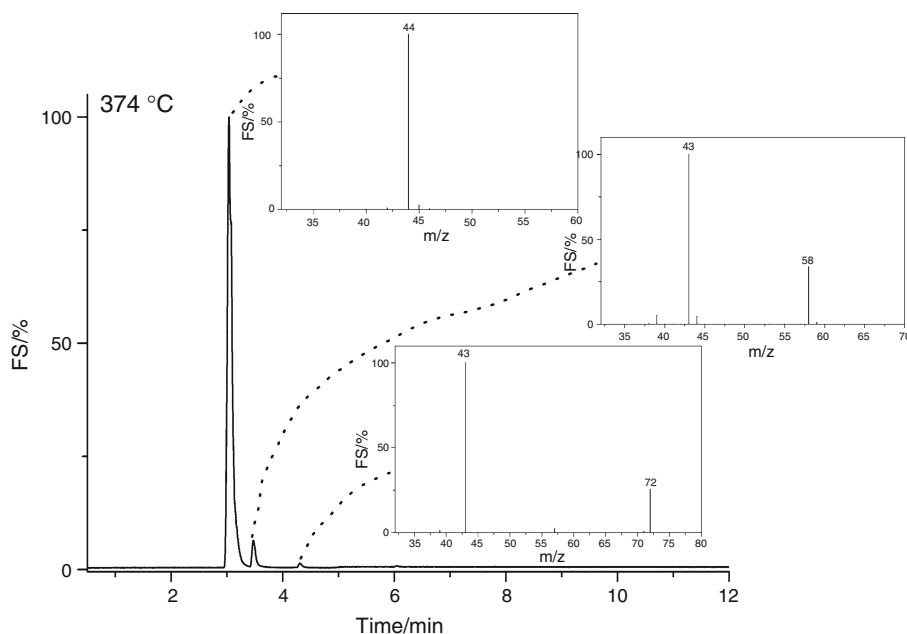

Fig. 8 TG/DTG curves of the Ho–O precursor gel under flowing nitrogen

is clearly seen that the single-phase holmium iron garnet is obtained.

For the better understanding of the formation of the end product, thermal behaviour of Ho–Fe–O gel was investigated. TG, DTG and DSC curves of Ho–Fe–O precursor gel carried out in the flowing air are shown in Fig. 2. As can be seen from the DTG curve, thermal behaviour of the gel is related to the four different mass loss steps centred at 110, 205, 358 and 765 °C. First mass loss step at 110 °C is mainly related to the release of water, which is probably trapped inside the porous gel network. This is also evident from the broad endothermic signal in the DSC curve. The second mass loss step observed in the range of around 160–260 °C is accompanied by an exothermic peak with the maxima at 233 °C. This can be assigned to the

beginning of the decomposition of the organic part with the formation of intermediate species [26]. Mass loss and sharp exothermic peak at 363 °C in the DSC curve can be attributed to the decomposition of formed complexes during the gelation process [27], burning of weakly bound organic groups [23] and loss of coordinated ethylene glycol [28]. For similar garnet structure compounds, mass loss at around 765 °C indicates complete transformation from the complex type compound to the mixed-metal oxide [29]. These results are in good agreement with the XRD analysis results, which showed the formation of the single-phase holmium iron garnet at 800 °C.

The pyrolysis of Ho–Fe–O precursor gel was also investigated by TG–GC–MS analysis. Figure 3 shows TG and DTG curves of the Ho–Fe–O precursor gel under flowing nitrogen. As compared to the TG curve obtained in the air, the first two steps of mass loss occur almost in the same temperature, while third step has the maxima at higher temperature (415 °C). On the other hand, the last mass loss step occurs at lower temperature (656 °C).

Sampling of the evolved gas phase for TG–GC–MS analysis was performed at 415 and 656 °C in order to better identify compounds released during thermal decomposition process. Gas chromatographic elutions carried out at 415 and 656 °C are reported in Fig. 4. As shown in Fig. 4, the release of CO_2 (m/z signal at 44) and acetone CH_3COCH_3 (m/z signals at 43 for CH_3CO^+ ion and at 58 for $CH_3COCH_3^+$) is detected at 415 °C. Evolution of these species is related to the decomposition of organic part of intermediate complex gel network. On the contrary, only CO_2 signal (m/z at 44) is detected at higher thermal decomposition temperature (656 °C). As was mentioned

Fig. 9 Gas chromatographic elutions of the gas phase evolved at 132 °C of Ho–O gel under flowing nitrogen. Mass spectra recorded corresponding to selected chromatographic peaks (TG–GC–MS analysis)
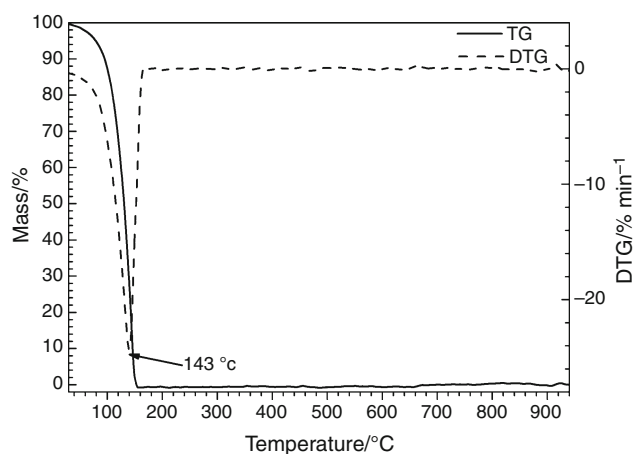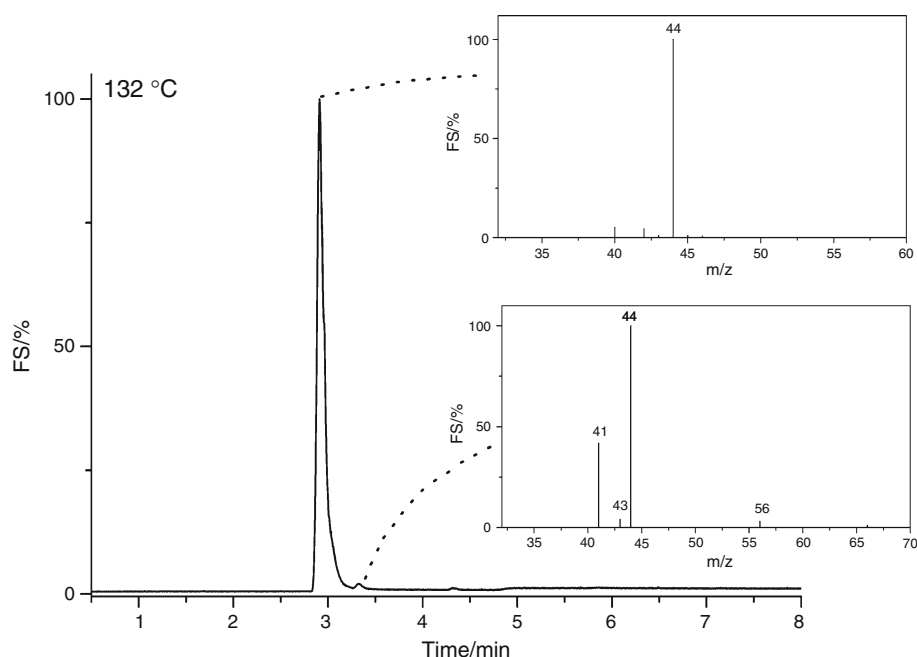

Fig. 10 TG/DTG curves of the 1,2-ethanediol under flowing nitrogen

before, the formation of mixed-metal oxide occurs at the temperature related to the final mass loss (656 °C). The release of CO_2 can be attributed to the decomposition of intermediates species such as oxycarbonates.

Figure 5 demonstrates the decomposition products at the main DTG peak of Ho–Fe–O precursor gel under flowing air. The main signal is assigned to the release of CO_2. In the presence of oxygen only CO_2 signal is seen, since the combustion of organic part occurs in the TG chamber. Only negligible amount of acetone CH_3COCH_3 (m/z signals at 43 for CH_3CO^+ ion and at 58 for $CH_3COCH_3^+$) is detected. The gel also contains nitrates, but decomposition of nitrates has to take place at lower temperatures. TG–GC–MS experiments of the lower temperature gases were not performed.

In order to better understand the decomposition of binary Ho–Fe–O precursor gel, the individual Fe–O and Ho–O gels were synthesized and investigated by TG–GC–MS. TG/DTG curves of Fe–O gel are shown in Fig. 6. Clearly, the main decomposition process of Fe–O gel occurs at 374 °C. Gas chromatographic elution was performed at this temperature, and the results are presented in Fig. 7. Obviously, the main released decomposition product is CO_2 (m/z signal at 44), whereas the compounds detected in the lower content are CH_3COCH_3 (m/z signals at 43 for CH_3CO^+ ion and 58 for $CH_3COCH_3^+$ ion) and $C_2H_5COCH_3$ (m/z signals at 43 for CH_3CO^+ ion and 72 for $C_2H_5COCH_3^+$ ion). The TG/DTG curves of Ho–O gel are shown in Fig. 8. Thermal decomposition of Ho–O gel also occurs via one mass loss step at 132 °C. At this temperature obtained the gas chromatogram (Fig. 9) presents few signals. The main release belongs to CO_2 (m/z signal at 44). In summary, evolved gases from Fe–O and Ho–O gels are the same as were determined during the decomposition of the Ho–Fe–O gel, except the small amount of $C_2H_5COCH_3$ (m/z signals at 43 for CH_3CO^+ ion and 72 for $C_2H_5COCH_3^+$ ion). TG–GC–MS measurements of Fe–O and Ho–O gels under flowing air showed release of CO_2 (m/z signal at 44) and confirmed burning of weakly bound organic groups as in the case of the Ho–Fe–O gel.

In the sol–gel processing, the 1,2-ethanediol was used as the complexing agent. In order to understand better the formation of the complexes, the TG–GC–MS analysis of the 1,2-ethanediol was also performed (see Figs. 10, 11). Apparently, thermal decomposition of the complexing agent occurs through one mass loss step at 143 °C. Main

Fig. 11 Gas chromatographic elutions of the gas phase evolved at 143 °C of 1,2-ethanediol under flowing nitrogen. Mass spectra recorded corresponding to selected chromatographic peaks (TG–GC–MS analysis)
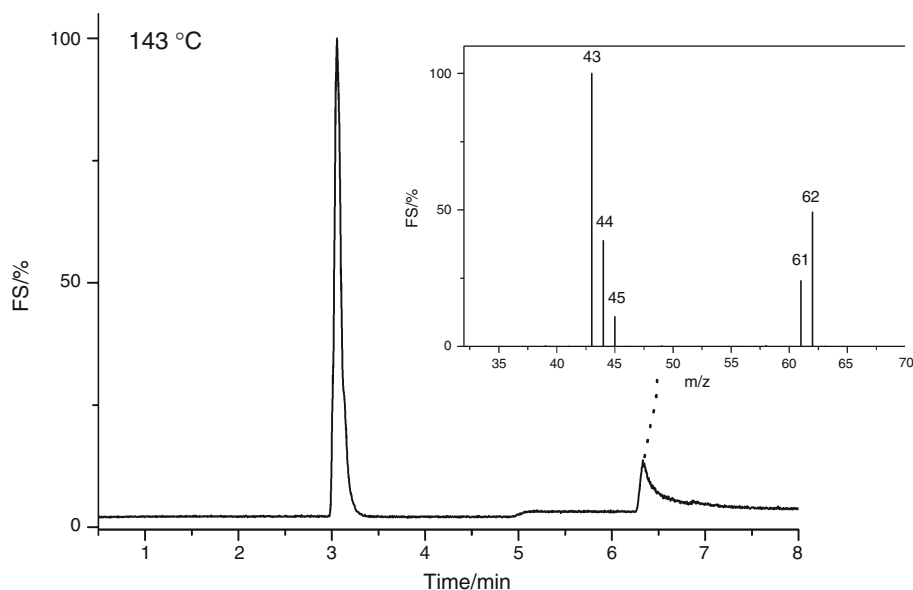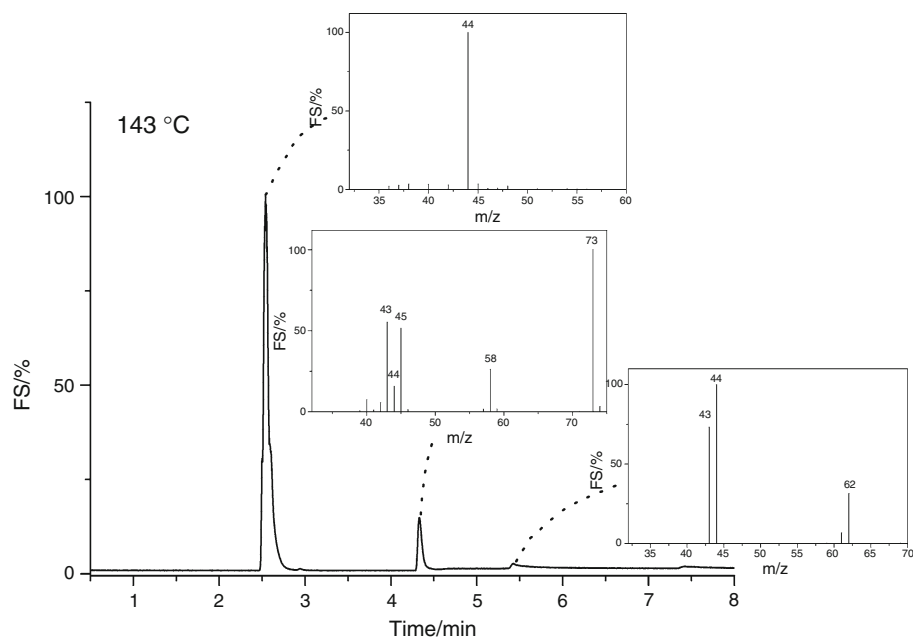

Fig. 12 Gas chromatographic elutions of the gas phase evolved at 147 °C of 1,2-ethanediol under flowing air. Mass spectra recorded corresponding to selected chromatographic peaks (TG–GC–MS analysis)

m/z signals are detected at 43 and 62. Figure 12 presents decomposition products of 1,2-ethanediol under flowing air. It is clearly seen that the released products are slightly different. Besides CO_2 (m/z signal at 44) and 1,2-ethanediol (m/z signals at 43 and 62), 2-methyl-1,3-dioxolane is released (m/z signals at 73, 43, 45, 58 and 62). In comparison with all previously analysed gels, these signals were not detected before, showing that 1,2-ethanediol obviously forms coordination compounds with the metal ions during the formation of the gel network. Interestingly, the individual Fe–O and Ho–O gels as well as 1,2-ethanediol decomposed at lower temperatures in comparison with the bimetallic Ho–Fe–O gel. This observation let

us to conclude that the binary Ho–Fe–O gel is more thermally stable.

Mössbauer spectroscopy and Curie temperature

The $Ho_3Fe_5O_{12}$ prepared by an aqueous sol–gel method at 800 °C was monitored by Mössbauer spectroscopy. Room-temperature Mössbauer spectra of HoIG are depicted in Fig. 13. It is clearly seen that obtained spectra well fit with two magnetic subspectra (sextets) which correspond to non-equivalent octahedral and tetrahedral positions in the garnet structure. Isomeric shift of 0.38 mm s^{-1} and hyperfine field of 48.64 T are related to the Fe^{3+} ion in the
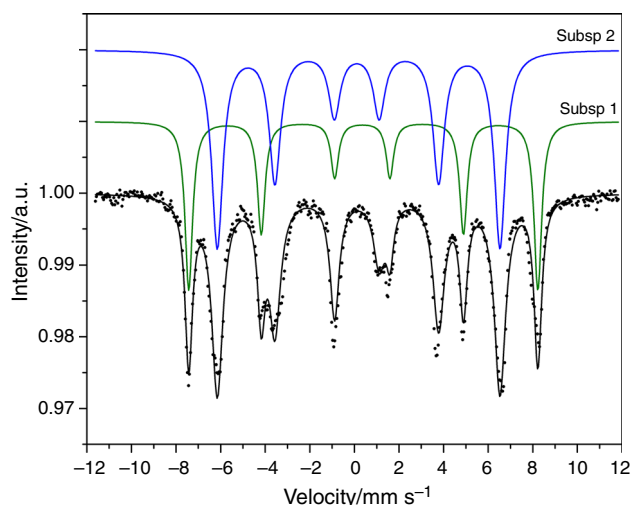
Fig. 13 Mössbauer spectra of $Ho_3Fe_5O_{12}$

Fig. 14 Mass change of $Ho_3Fe_5O_{12}$ samples synthesized at 800, 900 and 1000 °C under external magnetic field

octahedral site, while isomeric shift of 0.15 mm s^{-1} and hyperfine field of 39.38 T are related to the Fe^{3+} ion in the tetrahedral site (Table 1). These hyperfine parameters correspond well to those stated previously for similar garnet structure compounds [23, 30].

Mössbauer spectroscopy is an important tool not only for the determination of hyperfine parameters, but also for the evaluation of the distribution of Fe^{3+} ions among sublattices of garnet structure. For single-phase holmium iron garnet, the area ratio of subspectra attributable to 24d tetrahedral and 16a octahedral sites slightly exceeds the 3:2 (Table 1).

It is known that thermal analysis is an alternative way to determine Curie temperature [6, 7, 9]. Thermogravimetry with adapted small magnet was used to determine Curie temperature of holmium iron garnet samples annealed at 800, 900 and 1000 °C and other rare earth iron garnets. From the obtained thermomagnetic curves, the transition temperature from ferrimagnetic to paramagnetic state was observed. Figure 14 shows determined Curie temperature for $Ho_3Fe_5O_{12}$ obtained at different temperatures. Onset calculation was made at the end of the Curie point transition (Fig. 14 $Ho_3Fe_5O_{12}$ annealed at 800 °C). Obviously, Curie temperature of holmium iron garnet samples prepared at various temperatures is almost the same, even the determined phase composition is slightly different. $Ho_3Fe_5O_{12}$ garnet annealed at 1000 °C has small impurities of perovskite-type $HoFeO_3$, while garnet phase is dominant
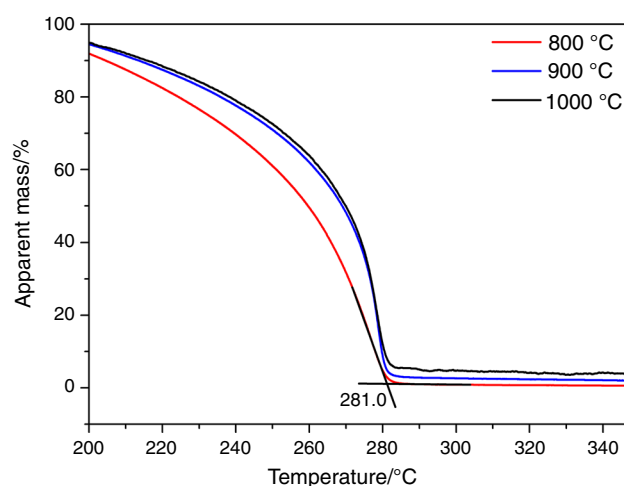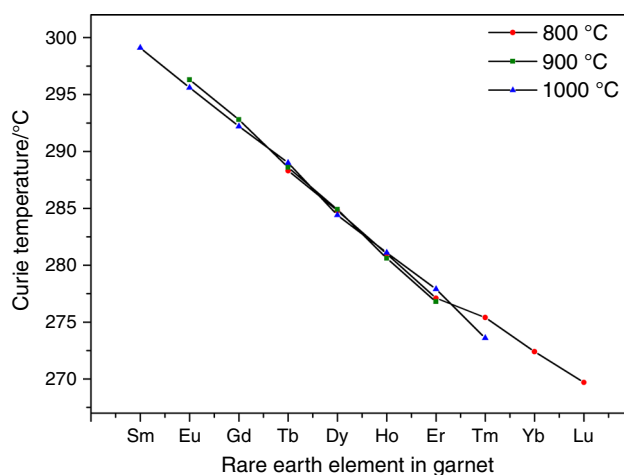

Fig. 15 Curie temperature dependence of rare earth element in the garnet

for the sample annealed at 900 °C, but amount of $HoFeO_3$ is even higher [25]. For the $Ho_3Fe_5O_{12}$ garnet annealed at 800 °C Curie temperature is 281.0 °C, for synthesized at 900 is 280.6 °C, and for synthesized at 1000 is 281.1 °C. The lowest Curie point was determined for the $Ho_3Fe_5O_{12}$ sample prepared at 900 °C, which has the highest amount of side phase. In conclusion, we can say that small amount of impurity phase does not affect the value of Curie point significantly.

Table 1 Data from Mössbauer spectra measured at room temperature

	Isomer shift δ/mm s^{-1}	Quadrupole splitting ΔE_Q/mm s^{-1}	Hyperfine field B_{Hf}/T	Full line width at half height/mm s^{-1}	Relative area/%	Interpretation
Subsp. 1	0.38	0.04	48.64	0.41	36.28	Fe^{3+} in octahedral position in HoIG
Subsp. 2	0.15	0.08	39.38	0.62	63.72	Fe^{3+} in tetrahedral position in HoIG

Further, Curie temperatures of other rare earth iron garnets were determined by the same way. Temperature dependence of Curie temperatures for the rare earth elements in the iron garnet is shown in Fig. . As seen, in the series of lanthanide ions from Sm^{3+} to Lu^{3+} Curie temperature monotonically decreases. Clearly, the nature of rare earth ion in the iron garnet affects the value of Curie temperature allowing to choose desirable Curie temperature by selecting the particular lanthanide iron garnet.

Conclusions

The formation of monophasic holmium iron garnet ($Ho_3Fe_5O_{12}$, HoIG) during an aqueous sol–gel processing was investigated by combined TG–GC–MS analysis. It was shown that Ho–Fe–O precursor gel has been formed through intermediate coordination compounds. The higher thermal stability of binary Ho–Fe–O gel in comparison with individual Fe–O and Ho–O gels was also determined. The thermal decomposition products CO_2 and acetone (CH_3COCH_3) were identified in the case of Ho–Fe–O gel under flowing nitrogen. However, the CO_2, acetone and 2-butanone ($C_2H_5COCH_3$), or mainly CO_2 released during the decomposition of individual Fe–O and Ho–O gel, respectively. TG–GC–MS measurements under flowing air showed the CO_2 as the main decomposition product of all gels. Mössbauer spectroscopy of $Ho_3Fe_5O_{12}$ garnet showed that at room temperature this material prefers magnetically ordered structure. Curie temperature determined by adapted thermal analyser allowed us to identify that the transition from ferrimagnetic to paramagnetic state of holmium iron garnet occurs at 281 °C. Curie temperature for the series of sol–gel chemistry derived rare earth iron garnets was also determined. It was shown that Curie temperature monotonically decreased in the series from Sm^{3+} to Lu^{3+}. In conclusion, the selection of lanthanide element in rare earth iron garnets leads to the desirable final product with preferable magnetic properties.

References

1. Suchomski C, Reitz C, Pajic D, Jaglicic Z, Djerdj I, Brezesinski T. Large-pore mesoporous $Ho_3Fe_5O_{12}$ thin films with a strong room-temperature perpendicular magnetic anisotropy by sol–gel processing. Chem Mater. 2014;26:2337–43.

2. Harris IR, Williams AJ. Magnetic materials. In: Rawlings RD, editor. Material science and engineering, vol. 2. Oxford: Eolls Publishers; 2009. p. 49–84.

3. Callister WD, Rethwisch DG. Materials science and engineering: an introduction. 9th ed. London: Wiley; 2013.

4. Coey JMD. Magnetism and magnetic materials. New York: Cambridge University Press; 2009.

5. Dobrzański LA, Drak M, Ziębowicz B. Materials with specific magnetic properties. J Achiev Mater Manuf Eng. 2006;17:37–40.

6. Suñol JJ, González A, Escoda L, Vilaró A. Curie temperature in Fe(Ni)Nb based mechanically alloyed materials. J Therm Anal Calorim. 2005;80:257–61.

7. Lin DM, Lin ML, Lin MH, Wu YC, Wang HS, Chen YJ. Studies of nanocrystalline phase and residual amorphous phase of FeCuNbSib alloy using TG(M) technique. J Therm Anal Calorim. 1999;58:355–62.

8. Brown ME. Introduction to thermal analysis: techniques and applications. London: Chapman and Hall; 1988.

9. Luciani G, Costantini A, Branda F, Scardi P, Lanotte L. Thermal evolution of ferromagnetic metallic glasses. J Therm Anal Calorim. 2003;72:105–11.

10. Boyanov BS. Synthesis and neel temperature determination of ferrites from the $CuO–ZnO–Fe_2O_3$ system. J Therm Anal. 1995;44:707–16.

11. Sugimoto M. The past, present, and future of ferrites. J Am Ceram Soc. 1999;82:269–80.

12. Caffarena VR, Ogasawara T. Microstructure and hysteresis curves of samarium-holmium-iron garnet synthesized by coprecipitation. Mater Res. 2003;6:569–76.

13. Caffarena VR, Ogasawara T, Pinho MS, Capitaneo JL. Samarium-iron garnet nanopowder obtained by co-precipitation. Latin Am Appl Res. 2006;36:137–40.

14. Cheng Z, Yang H. Synthesis and magnetic properties of Sm–$Y_3Fe_5O_{12}$ nanoparticles. Phys E. 2007;39:198–202.

15. Ramesh T, Shinde RS, Murthy SR. Nanocrystalline gadolinium iron garnet for circulator applications. J Magn Magn Mater. 2012;324:3668–73.

16. McCloy JS, Walsh B. Sublattice magnetic relaxation in rare earth iron garnets. Trans Magn IEEE. 2013;49:4253–6.

17. Nguyet DTT, Duong NP, Satoh T, Anh LN, Hien TD. Magnetization and coercivity of nanocrystalline gadolinium iron garnet. J Magn Magn Mater. 2013;332:180–5.

18. Suchomski C, Reitz C, Sousa CT, Araujo JP, Brezesinski T. Room temperature magnetic rare-earth iron garnet thin films with ordered mesoporous structure. Chem Mater. 2013;25:2527–37.

19. Brinker CJ, Scherer GW. Sol–gel science: the physics and chemistry of sol–gel processing. San Diego: Academic Press; 1990.

20. Di Maggio R, Campostrini R, Guella G. Gels from modified zirconium n-butoxide: a pyrolysis study by coupled thermogravimetry, gas chromatographic, and mass spectrometric analyses. Chem Mater. 1998;10:3839–47.

21. Egger P, Dirè S, Ischia M, Campostrini R. Pyrolysis study of sol–gel derived zirconia by TG–GC–MS. J Therm Anal Calorim. 2005;81:407–15.

22. Oja Açik I, Madarász J, Krunks M, Tõnsuaadu K, Janke D, Pokol G, Niinistö L. Thermoanalytical studies of titanium(IV) acetylacetonate xerogels with emphasis on evolved gas analysis. J Therm Anal Calorim. 2007;88:557–63.

23. Pinkas J, Reichlova V, Serafimidisova A, Moravec Z, Zboril R, Jancik D, Bezdicka P. Sonochemical synthesis of amorphous yttrium iron oxides embedded in acetate matrix and their controlled thermal crystallization toward garnet ($Y_3Fe_5O_{12}$) and perovskite ($YFeO_3$) nanostructures. J Phys Chem C. 2010;114:13557–64.

24. Xie W, Pan W-P. Thermal characterization of materials using evolved gas analysis. J Therm Anal Calorim. 2001;65:669–85.

25. Opuchovic O, Kareiva A, Mazeika K, Baltrunas D. Magnetic nanosized rare earth iron garnets $R_3Fe_5O_{12}$: sol–gel fabrication, characterization and reinspection. J Magn Magn Mater. 2016;. doi:10.1016/j.jmmm.2016.09.041.

26. Masoudpanah SM, Mirkazemi SM, Shabani S, Dolat Abadi PT. The effect of the ethylene glycol to metal nitrate molar ratio on the phase evolution, morphology and magnetic properties of single phase $BiFeO_3$ nanoparticles. Ceram Int. 2015;41: 9642–6.

27. Opuchovic O, Beganskiene A, Kareiva A. Sol–gel derived $Tb_3Fe_5O_{12}$ and $Y_3Fe_5O_{12}$ garnets: synthesis, phase purity, microstructure and improved design of morphology. J Alloys Compd. 2015;647:189–97.

28. Wang Y, Jiang X, Xia Y. A solution-phase, precursor route to polycrystalline SnO_2 nanowires that can be used for gas sensing under ambient conditions. J Am Chem Soc. 2003;125:16176–7.

29. Arun T, Vairavel M, Gokul Raj S, Justin JR. Crystallization kinetics of Nd-substituted yttrium iron garnet prepared through sol–gel auto-combustion method. Ceram Int. 2012;38:2369–73.

30. Lataifeh M, Lehlooh AF, Mahmood S. Mössbauer spectroscopy of Al substituted Fe in holmium iron garnet. Hyperfine Interact. 1999;122:253–8.